JACS
JOURNAL OF THE AMERICAN CHEMICAL SOCIETY
pubs.acs.org/JACS
Article

Crystallographic Characterization of U@C_{2n} ($2n$ = 82−86): Insights about Metal−Cage Interactions for Mono-metallofullerenes

Yang-Rong Yao,[§] Yannick Roselló,[§] Lei Ma, Alain Rafael Puente Santiago, Alejandro Metta-Magaña, Ning Chen, Antonio Rodríguez-Fortea, Josep M. Poblet,* and Luis Echegoyen*

Cite This: *J. Am. Chem. Soc.* 2021, 143, 15309−15318
Read Online
ACCESS | Metrics & More | Article Recommendations | Supporting Information

ABSTRACT: Endohedral mono-metallofullerenes are the prototypes to understand the fundamental nature and the unique interactions between the encapsulated metals and the fullerene cages. Herein, we report the crystallographic characterizations of four new U-based mono-metallofullerenes, namely, U@C_s(6)-C_{82}, U@C_2(8)-C_{84}, U@C_s(15)-C_{84}, and U@C_1(12)-C_{86}, among which the chiral cages C_2(8)-C_{84} and C_1(12)-C_{86} have never been previously reported for either endohedral or empty fullerenes. Symmetrical patterns, such as indacene, sumanene, and phenalene, and charge transfer are found to determine the metal positions inside the fullerene cages. In addition, a new finding concerning the metal positions inside the cages reveals that the encapsulated metal ions are always located on symmetry planes of the fullerene cages, as long as the fullerene cages possess mirror planes. DFT calculations show that the metal−fullerene motif interaction determines the stability of the metal position. In fullerenes containing symmetry planes, the metal prefers to occupy a symmetrical arrangement with respect to the interacting motifs, which share one of their symmetry planes with the fullerene. In *all* computationally analyzed fullerenes containing at least one symmetry plane, the actinide was found to be located on the mirror plane. This finding provides new insights into the nature of metal−cage interactions and gives new guidelines for structural determinations using crystallographic and theoretical methods.

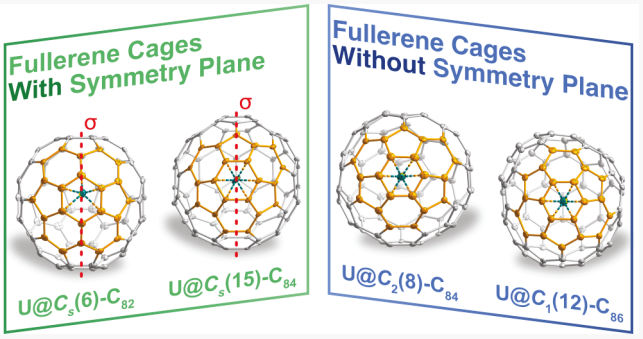

INTRODUCTION

Endohedral metallofullerenes (EMFs) are an interesting class of hybrid compounds for which different kinds of metal atoms or metallic clusters are encapsulated inside the interior of fullerene cages of various sizes.[1−3] In the past three decades, EMFs have attracted considerable interest due to their attractive properties, including the nature of the metal−cage interactions that are key to understanding the nature of EMFs and exploring their potential applications.[4−6] For example, very recently, Zhang et al. reported a single-molecule electret device based on Gd@C_{82} for the first time, proving that the encapsulated Gd atom hopping between two different sites inside the C_{82} cage results in two states with different permanent electrical dipole orientations.[7]

Since the first observation of La@C_{60} using mass spectroscopy in 1985, mono-metallofullerenes encapsulating single metal ions became the prototypes to understand the intermolecular interactions between the encapsulated metal and the fullerenes cages.[8] The characterization of Y@C_{82} using synchrotron radiation powder X-ray diffraction combined with Rietveld treatment and the maximum entropy method confirmed that the Y ion is located close to the carbon cage with strong metal−cage interactions instead of in the center of the fullerene cage.[9] The development of cocrystallization methods using metal porphyrins, which improve the crystallinity and inhibit the rotation of the fullerene cages, makes the structural studies of EMFs much easier and more accurate.[10] Up to now, mono-metallofullerenes containing various metal elements, including alkaline-earths,[11,12] rare-earths,[12−32] and actinides,[33−39] have been crystallographically characterized.

However, severe disorder is frequently observed in EMF cocrystals, especially for the encapsulated metal due to the motion inside the fullerene cage, which decreases the precision when determining the exact position of the metal and the corresponding metal−cage interactions. The cocrystals are commonly found in the *C*2/*m* space group, resulting in crystallographic mirror-related cage and metal orientations. In such cases, it is necessary to perform theoretical calculations for the optimized structures because the encapsulated metal ions and their mirror-related counterparts are generally

Received: July 1, 2021
Published: September 13, 2021

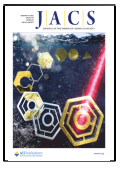

https://doi.org/10.1021/jacs.1c06833
J. Am. Chem. Soc. 2021, 143, 15309−15318

crystallographically indistinguishable, especially when they are highly disordered.

On the other hand, it is challenging to develop general rules governing the metal−cage interactions for mono-metallofullerenes because the metal positions change depending on the fullerene cage. For example, for M@C_{2v}(9)-C_{82} (M = lanthanide and U),[14−20] the metal is generally situated on the C_2 axis, while for M@C_{2v}(3)-C_{80} (M = Sm, Yb, and Eu)[25−28] with the same cage symmetry as M@C_{2v}(9)-C_{82}, the metal is not on the C_2 axis. Trying to understand the reasons for these observations should provide fundamental insights about the nature of the metal−cage interactions and the formation of the EMFs.

Herein, we report the successful synthesis, isolation, and characterization of four new mono-metallofullerenes U@C_{2n} ($2n$ = 82−86), namely, U@C_s(6)-C_{82}, U@C_2(8)-C_{84}, U@C_s(15)-C_{84}, and U@C_1(12)-C_{86}. Notably, the C_2(8)-C_{84} and C_1(12)-C_{86} cages have never been reported before, either as empty fullerenes or as EMFs, and C_s(15)-C_{84} was found to be stabilized by a single U ion for the first time. Most importantly, based on the crystallographic identification of C_s(6)-C_{82} and C_s(15)-C_{84}, a general observation that applies for all the mono-metallofullerenes was serendipitously found, showing that the metal is always situated on the symmetry planes for fullerene cages that possess mirror planes. This general observation is not dependent on the metal type, cage size, and cage motif coordinated with the metal ion. A careful DFT analysis for a series of U@C_{2n} endofullerenes has allowed us to show that the metal always prefers to occupy a symmetrical arrangement with respect to the interacting motifs, which share one of their mirror planes with the carbon cage, as long as the fullerene possesses mirror planes.

RESULTS AND DISCUSSION

Synthesis and Isolation of U@C_{2n} ($2n$ = 82−86). U@C_{2n} ($2n$ = 82−86) were synthesized by the direct-current arc-discharge method under optimized conditions. High-purity graphite rods filled with a mixture of U_3O_8/graphite powder (molar ratio of U/C = 1/24) were evaporated in an arcing reactor under a 200 Torr He atmosphere. The resulting soot was soaked in a CS_2 solution overnight and then extracted in a supersonic cleaner for 1 h. Multiple-stage high-performance liquid chromatography (HPLC) procedures were employed to purify the four new fullerenes (see details in Figures S1−S4). The retention time of the new U@C_{82} isomer is between its two isomers, U@C_{2v}(9)-C_{82} and U@C_2(5)-C_{82},[36] on a Buckyprep column. For U@C_{84} and U@C_{86}, U@C_{84} (I) and U@C_{84} (II) both exhibit longer retention times than U@D_2(21)-C_{84}, while U@C_{86} has a shorter retention time than the two previously reported U@C_{86} isomers, U@C_s(15)-C_{86} and U@C_1(11)-C_{86}, on a Buckyprep column.[38] The high purities of the four new compounds were confirmed by the observation of single peaks by HPLC and the corresponding positive-ion mode matrix-assisted laser desorption ionization time-of-flight (MALDI-TOF) mass spectra, as shown in Figure 1. In addition, the experimental isotopic distributions were found to be in perfect agreement with the theoretical predictions.

Crystallographic Characterization of U@C_{2n} ($2n$ = 82−86). Single crystals of the four U@C_{2n} ($2n$ = 82−86) were obtained by cocrystallization with Ni^{II}(OEP) (OEP = 2, 3, 7, 8, 12, 13, 17, 18-octaethylporphyrin dianion). The molecular structures of U@C_{82}, U@C_{84} (I), U@C_{84} (II), and U@C_{86} were unambiguously determined as U@C_s(6)-C_{82}, U@C_2(8)-C_{84}, U@C_s(15)-C_{84}, and U@C_1(12)-C_{86}, respectively, by X-ray crystallography, as shown in Figure 2. The detailed crystallographic information is listed in Table S1. The C_s(6)-C_{82} cage has been reported for lanthanide-based mono-metallofullerenes with metallic oxidation states of +2 or +3 and for some di-metallofullerenes and clusterfullerenes exhibiting a four-electron transfer to the cage, such as Sc_2X@C_s(6)-C_{82} (X = C_2, O, S)[40−42] and M_2@C_s(6)-C_{82} (M = Y, Er, Lu).[43−45] For U@C_s(15)-C_{84}, to the best of our knowledge, this is the first observation that the C_s(15)-C_{84} cage is stabilized by one metal

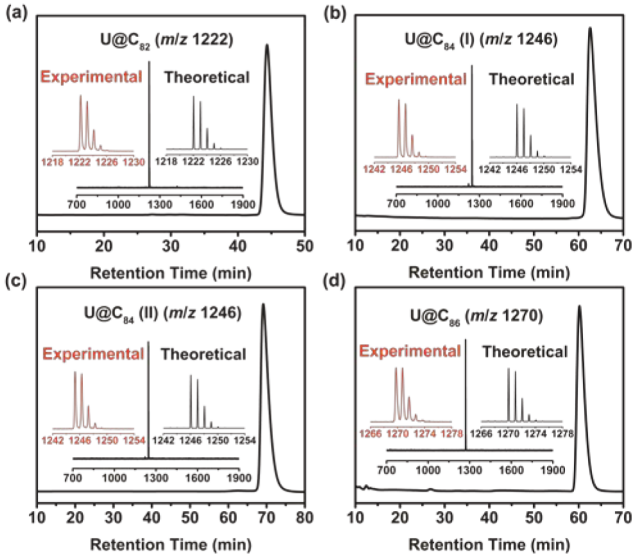

Figure 1. HPLC chromatograms of purified (a) U@C_{82}, (b) U@C_{84} (I), (c) U@C_{84} (II), and (d) U@C_{86} on a semipreparative Buckyprep column at a flow rate of 4 mL/min using toluene as the eluent. Insets show the corresponding MALDI-TOF mass spectra with expansion comparisons between the experimental and theoretical isotopic distributions.

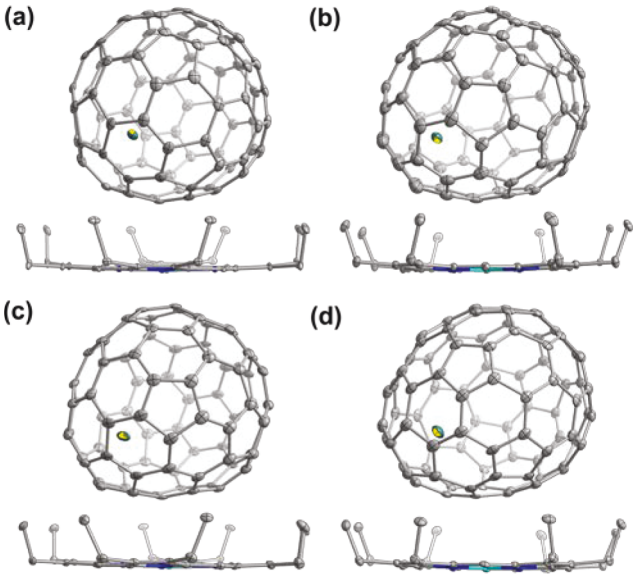

Figure 2. Oak ridge thermal ellipsoid plot (ORTEP) drawings of (a) U@C_s(6)-C_{82}, (b) U@C_2(8)-C_{84}, (c) U@C_s(15)-C_{84}, and (d) U@C_1(12)-C_{86} cocrystallized with Ni^{II}(OEP). For clarity, only the major orientation of the cage and U site is shown, and all the solvent molecules and hydrogen atoms are omitted.

https://doi.org/10.1021/jacs.1c06833
J. Am. Chem. Soc. 2021, 143, 15309−15318

ion, and it was only reported for $Er_2C_2@C_s(15)$-C_{84} previously.[46] Notably, $C_2(8)$-C_{84} and $C_1(12)$-C_{86} are new cages that have never been reported before either as empty fullerenes or as EMFs, showing that U has unique electronic properties that stabilize unstable fullerene cages.

The cocrystallized Ni^{II}(OEP) molecules play an essential role in improving the crystallization and inhibiting the fullerene cages' rotations. The closest contacts between the nickel atom and the cage carbon of the four fullerenes were measured as 2.83, 2.93, 2.89, and 2.98 Å for $U@C_s(6)$-C_{82}, $U@C_2(8)$-C_{84}, $U@C_s(15)$-C_{84}, and $U@C_1(12)$-C_{86}, respectively, suggesting substantial $\pi-\pi$ interactions between the fullerene cages and the Ni^{II}(OEP) molecules. Interestingly, all of the cocrystals show a remarkable degree of consistency with the encapsulated metal close to the porphyrin plane. Such orientations are likely affected by the neighboring metalloporphyrin through charge transfer between the encapsulated U and the cage, resulting in a relatively negative cage section that can interact via $\pi-\pi$ interactions with the metallic porphyrin molecule.

The crystallographic analysis shows that the cocrystals crystallized in the monoclinic space group $C2/m$ for $U@C_s(6)$-C_{82} and $U@C_2(8)$-C_{84} and the triclinic space group $P\bar{1}$ for $U@C_s(15)$-C_{84} and $U@C_1(12)$-C_{86}. These two space groups are commonly found in many analogous EMF/Ni^{II}(OEP) systems. In the cases of $U@C_s(6)$-C_{82} and $U@C_2(8)$-C_{84}, the fullerene cages show two orientations due to the crystallographic mirror of the $C2/m$ space group. An intact fullerene cage with an occupancy of 0.5 is combined by one-half of one orientation and the mirror-related half of the other orientation. Although no crystallographic mirror exists for the space group $P\bar{1}$, two disordered cage orientations are also observed with occupancies of 0.59/0.41 for $U@C_s(15)$-C_{84} and 0.54/0.46 for $U@C_1(12)$-C_{86}. As shown in Figure 3, inside the fullerene cages, the U ions for all four compounds also suffer from some disorder. For the crystals in the space group $C2/m$, the existence of the crystallographic mirror makes it challenging to determine the actual structures because the metal ions and their mirror-related counterparts are frequently indistinguishable.

Although four disordered U sites are observed for $U@C_s(15)$-C_{84}, the predominant U site (U1, 0.51) has a much higher occupancy than the minor sites. In addition, the less occupied orientations can be easily excluded because the closest U1−cage distance (2.01 Å) is electronically unreasonable and much shorter than previously reported U−cage contacts (2.3−2.4 Å). Similarly, seven disordered U sites are observed for $U@C_1(12)$-C_{86}, in which the primary U site (U1, 0.357) is much more occupied than the others. The relationship between U1 and the minor cage orientation was not considered due to the unreasonably short U−cage distance (2.07 Å). In conclusion, the most stable structures of these two EMFs can be unambiguously established crystallographically.

The situation is somewhat different for $U@C_s(6)$-C_{82} and $U@C_2(8)$-C_{84}. Inside the cage of $C_2(8)$-C_{84}, nine U positions with occupancies ranging from 0.029 to 0.227 were refined, among which U2 is situated in the crystallographic mirror, and $U1_m$, $U3_m$, $U4_m$, and $U5_m$ are generated by the crystallographic mirror plane. Additional analysis shows that even though the predominant sites U1 and $U1_m$ are identically occupied due to the crystallographic mirror plane, the closest distance between U1 and the cage is much more reasonable than that between $U1_m$ and the cage (2.28 Å versus 1.81 Å). For $U@C_s(6)$-C_{82}, among the seven observed U ion positions, only U4, with an occupancy of 0.02, is situated in the crystallographic mirror. $U1_m$, $U2_m$, and $U3_m$ are generated via their mirror-related counterparts, U1, U2, and U3, with occupancies of 0.377, 0.075, and 0.037, respectively. However, as shown in Figure 4, the closest U1−cage and $U1_m$−cage distances are identical (2.39 Å versus 2.38 Å) and are in agreement with previously reported mono-metallofullerenes. Therefore, in this case, U1

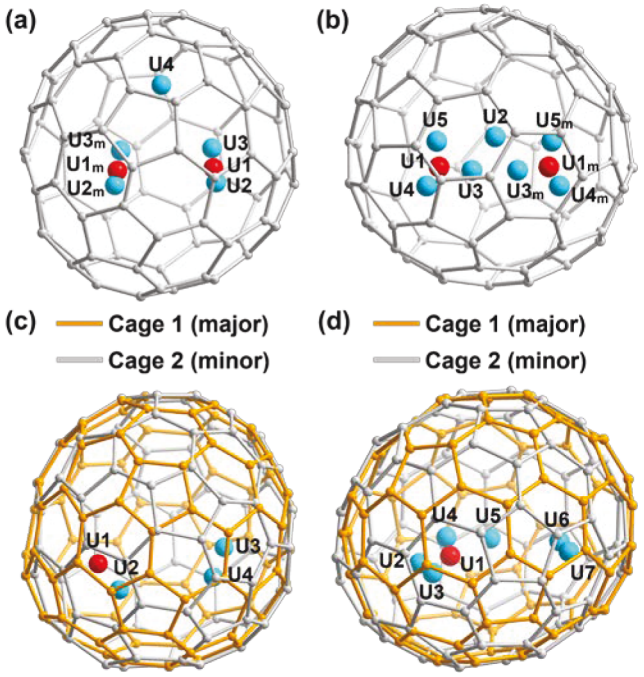

Figure 3. Diagram showing all of the disordered metal sites and cage orientations for (a) $U@C_s(6)$-C_{82}, (b) $U@C_2(8)$-C_{84}, (c) $U@C_s(15)$-C_{84}, and (d) $U@C_1(12)$-C_{86}. The U atom labeled with a subscript "m" is generated via the crystallographic mirror. The major U sites are highlighted in red, and the minor sites are shown in sky blue. For (c) $U@C_s(15)$-C_{84} and (d) $U@C_1(12)$-C_{86}, the major cage orientation is highlighted in orange, and the minor cage orientation is shown in light gray.

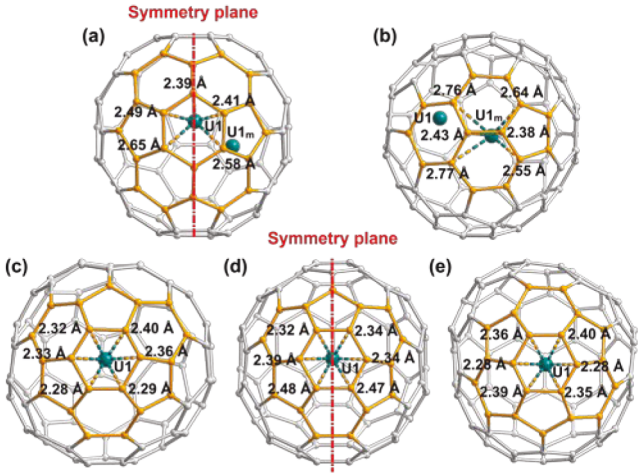

Figure 4. Diagrams showing the interactions of the predominant metal sites with the closest cage portions for (a) $U@C_s(6)$-C_{82} (U1), (b) $U@C_s(6)$-C_{82} ($U1_m$), (c) $U@C_2(8)$-C_{84}, (d) $U@C_s(15)$-C_{84}, and (e) $U@C_1(12)$-C_{86}. Symmetry planes are highlighted with dotted red lines. The fullerene cage segments closest to the encapsulated metal ions are highlighted in light orange.

https://doi.org/10.1021/jacs.1c06833
J. Am. Chem. Soc. 2021, 143, 15309−15318

and $U1_m$ are not crystallographically distinguishable to determine the actual structure of U@C_s(6)-C_{82}.

Further crystallographic analysis shows that U1 is located on the symmetry plane of the C_s(6)-C_{82} cage, while $U1_m$ is not. Generally, molecules naturally tend to be symmetric. Based on the crystallographic determination of U@C_s(15)-C_{84}, in which the primary metal site is also located on the symmetry plane, U1 seems intuitively more reasonable for U@C_s(6)-C_{82} since it preserves the molecular mirror plane. In addition, the U ions in U@C_2(8)-C_{84}, U@C_s(15)-C_{84}, and U@C_1(12)-C_{86} all reside in the center over a hexagon with the closest U−cage contacts within very narrow ranges of 2.28−2.40, 2.33−2.48, and 2.28−2.40 Å, respectively. Furthermore, all the closest hexagons are surrounded by three pentagons and three hexagons, forming unique sumanene-type structures, in excellent agreement with previous theoretical predictions for the Th@C_{2n} family,[47] suggesting the unique metal−cage interactions between actinide elements and fullerene cages.

Electronic Properties of U@C_{2n} ($2n$ = 82−86). The spectroscopic properties of the four purified U-based mono-metallofullerenes dissolved in toluene were investigated by visible−near-infrared (vis−NIR) absorption spectroscopy. As shown in Figure 5, U@C_s(6)-C_{82} shows three distinct

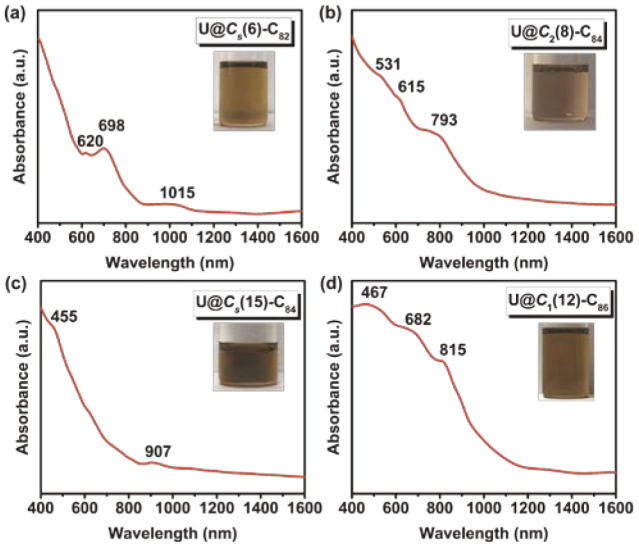

Figure 5. Vis−NIR absorption spectra of purified (a) U@C_s(6)-C_{82}, (b) U@C_2(8)-C_{84}, (c) U@C_s(15)-C_{84}, and (d) U@C_1(12)-C_{86} in toluene.

absorptions at 620, 698, and 1015 nm, different from those of its two isomers, U@C_{2v}(9)-C_{82} and U@C_2(5)-C_{82}. The two U@C_{84} isomers also have different absorption spectra compared with U@D_2(21)-C_{84}. U@C_2(8)-C_{84} displays three shoulder absorptions at 513, 618, and 793 nm, while U@C_s(15)-C_{84} shows two shoulder absorptions at 455 and 907 nm. Similarly, the absorption spectrum of U@C_1(12)-C_{86} is different from those of its two isomers, U@C_1(11)-C_{86} and U@C_s(15)-C_{86}, exhibiting a broad absorption in the range from 400 to 1200 nm with three shoulder peaks at 467, 682, and 815 nm. Interestingly, the absorption spectrum of U@C_s(6)-C_{82} is similar to those of other trivalent lanthanide-based M@C_s(6)-C_{82}, such as Y@C_s(6)-C_{82} and Er@C_s(6)-C_{82},[13,19] while U@C_s(15)-C_{84} shows distinct absorption features from those of Er_2C_2@C_s(15)-C_{84}.[46] In addition, the absorption features for U@C_2(8)-C_{84} and U@C_1(12)-C_{86} are unique because they correspond to new cages that have never been reported previously.

The electrochemical properties of U@C_{2n} ($2n$ = 82−86) were investigated by cyclic voltammetry (CV) with a three-electrode system in *ortho*-dichlorobenzene (*o*-DCB) solution using tetrabutylammonium hexafluorophosphate ($TBAPF_6$) as the supporting electrolyte. As shown in Figure 6, U@C_s(6)-C_{82}

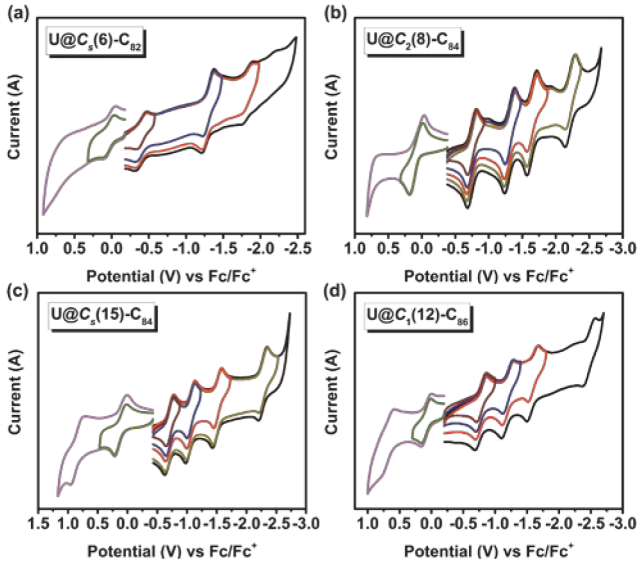

Figure 6. Cyclic voltammograms of (a) U@C_s(6)-C_{82}, (b) U@C_2(8)-C_{84}, (c) U@C_s(15)-C_{84}, and (d) U@C_1(12)-C_{86} in a 0.05 M $TBAPF_6$/*o*-DCB solution at a scan rate of 100 mV/s. Ferrocene (Fc) and $TBAPF_6$ were used as the internal standard and supporting electrolyte, respectively.

shows a distinct CV curve with a reversible oxidative step, three reversible reductive steps, and an irreversible reductive step. The first oxidation and reduction potentials are located at 0.04 and −0.41 V, respectively, resulting in a small electrochemical gap of 0.45 V, which is the smallest gap of all known U@C_{2n} compounds (Table S2).[36−38] Interestingly, the redox behavior of U@C_s(6)-C_{82} shows a resemblance to that of U@C_{2v}(9)-C_{82} with a similar small bandgap (0.53 V).

Unlike U@C_s(6)-C_{82}, all the redox processes of two U@C_{84} isomers and U@C_{86} are entirely reversible. U@C_s(15)-C_{84} and U@C_1(11)-C_{86} display four reductive and two oxidative processes, while for U@C_2(8)-C_{84}, only one single-electron oxidative step is observed. Interestingly, these three compounds also show very similar first oxidation and reductive potentials, resulting in similar electrochemical gaps. It should be noted that except for U@C_s(6)-C_{82} and U@C_{2v}(9)-C_{82}, the other 10 characterized U@C_{2n} ($2n$ = 74−86) compounds display similar electrochemical gaps ranging from 0.78 to 1.06 V, which may result from the unique redox behavior for the U@C_{2n} family if the reduction processes take place on the encapsulated U ion instead of on the carbon cage due to the low energies of the U 5f orbitals.[37]

Studies of Metal Positions in Mono-metallofullerenes. It is well-known that for non-IPR EMFs, the metal ions are always located over the fused pentagons due to strong metal−pentalene interactions, while for isolated pentagon rule (IPR) EMFs, the encapsulated metal ions are located over different cage segments.[48] However, on the basis of the crystallographic results for U@C_s(6)-C_{82} and U@C_s(15)-C_{84},

https://doi.org/10.1021/jacs.1c06833
J. Am. Chem. Soc. 2021, 143, 15309−15318

we wondered if the encapsulated metal ions are always located on symmetry planes of the fullerene cages, as long as the fullerene cages possess mirror planes. In order to gain a more fundamental understanding of metal−cage interactions, we reanalyzed the structures of published mono-metallofullerenes that have been reported from X-ray diffraction studies.[11−39] Except for M@I_h-$C_{60}(CF_3)_5$ (M = La and Gd),[49] La@D_{5h}-$C_{70}(CF_3)_3$,[50] and La@C_2(10612)-$C_{72}(C_6H_3Cl_2)$,[51] which were characterized in the form of derivatives, the crystallographically characterized mono-metallofullerenes with 30 different kinds of pristine cages are shown in Figure 7, among which 15

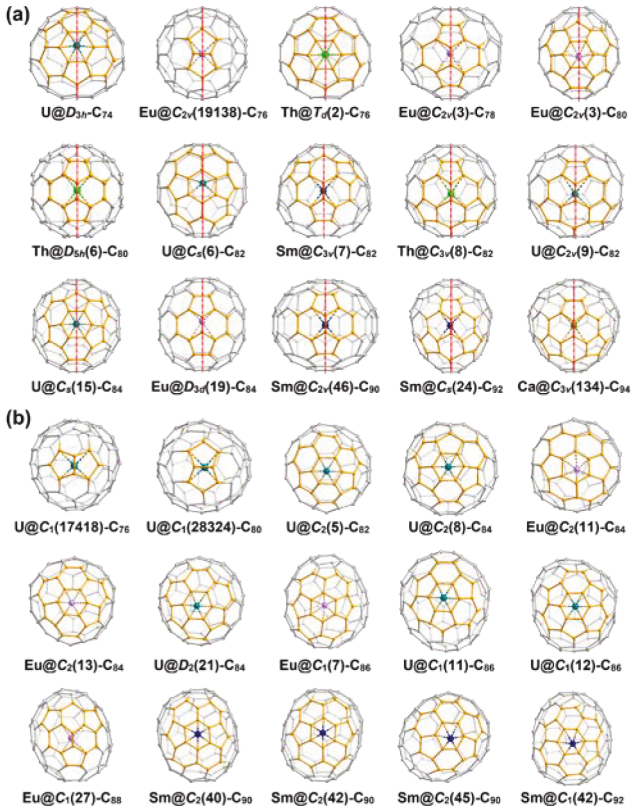

Figure 7. Molecular structures of crystallographically characterized mono-metallofullerenes with pristine cages that (a) contain symmetry planes and (b) do not contain symmetry planes. Symmetry planes are highlighted with dotted red lines. The fullerene cage segments closest to the encapsulated metal ions are highlighted in light orange.

possess cages with symmetry planes, and the other 15 do not. Notably, only one metal was selected to show when various metals were encapsulated in the same cage. For Sm@C_2(40)-C_{90} and Sm@C_2(42)-C_{90},[29] the actual structures are still not well established because of alternate orientations of the fullerene cages in the $C2/m$ space group and due to severe disorder of the metal positions with similar occupancies. Accordingly, only one reasonable possibility is shown for these two EMFs, and the other possibilities are shown in Figures S5 and S6.

Unsurprisingly, for non-IPR fullerenes, such as Eu@C_{2v}(19138)-C_{76}, U@C_1(17418)-C_{76}, and U@C_1(28324)-C_{80}, the metal ions are located over the [5, 5] bond. For IPR structures, the metal positions can be roughly divided into two types, over a hexagon or over a [6, 6] bond. Interestingly, most metal ions in fullerenes without symmetry planes prefer to reside over the center of a hexagon surrounded by two pentagons or three pentagons, including *as*-indacene-type, *s*-indacene-type, and sumanene-type hexagons. Compared to lanthanide ions, which typically reside over *as*-indacene-type or *s*-indacene-type hexagons, actinide ions are more likely to be positioned over sumanene-type hexagons, such as U@D_{3h}-C_{74}, Th@T_d(2)-C_{76}, U@C_2(8)-C_{84}, U@C_s(15)-C_{84}, U@C_1(11)-C_{86}, and U@C_1(12)-C_{86}. Notably, the sumanene-type pattern represents the closest way that pentagons can be together without violating the IPR rule. Another option for the encapsulated metal ions is to be situated over a [6, 6] bond, especially for cages with symmetry planes. For such metal−cage contacts, the metal ions are either over the center of a [6, 6] bond or close to a three-hexagon-junction (THJ) carbon. Accordingly, the [6, 6] bonds can be classified into two types, namely, *as*-indacene-type and phenalene-type [6, 6] bonds. The *as*-indacene-type and phenalene-type contacts between the metal ions and the [6, 6] bonds are both found for lanthanide-based and actinide-based mono-metallofullerenes. All the patterns are shown in Scheme 1.

Scheme 1. Different Patterns That Show the Metal−Cage Interactions in Mono-metallofullerenes

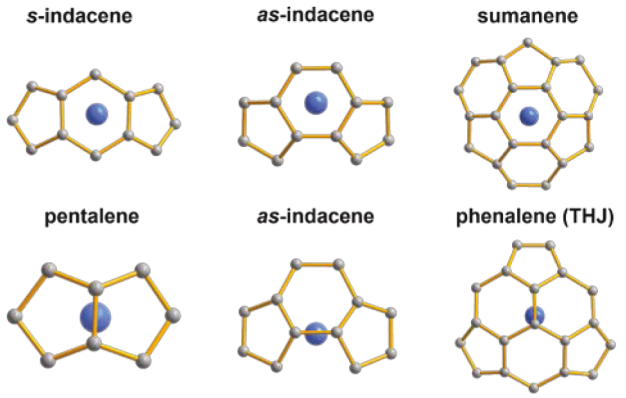

It is worth noting that when the fullerene cages possess mirror symmetry planes, the metal ions are always located on these symmetry planes. This observation applies for all mirror-symmetric mono-metallofullerenes, no matter what the metal is, what the fullerene size is, and what kind of fullerene segment is coordinated with the metal ion. Even for the non-IPR C_{2v}(19138)-C_{76}, the Eu ion is not only coordinated with the [5, 5] bond but also located on the symmetry plane. This finding gives a possible reason to explain the differences of coordinated fullerene patterns concerning the encapsulated metal ions between mirror-symmetric and non-mirror-symmetric cages. For the latter EMFs, the metal ions tend to be located over a hexagon pattern, while for mirror-symmetric cages, the symmetry planes are the most likely positions for the encapsulated metal ions. Therefore, besides the hexagon patterns, the [6, 6] bond patterns are commonly found for mirror-symmetric EMFs.

It should be noted that the charge transfer and the strength of metal−cage interactions between the encapsulated metal ions and the fullerene cages must also play an essential role in determining the position of the metal ions. For example, for M@D_{3h}-C_{74} (M = Ba, Eu, Sm, and U),[11,26,32,36] a four-electron transfer is only observed between the U ion and the cage, while the other metal ions all transfer two electrons to the cage, as shown in Figure 8. As a result, although all the metal ions are

https://doi.org/10.1021/jacs.1c06833
J. Am. Chem. Soc. 2021, 143, 15309−15318

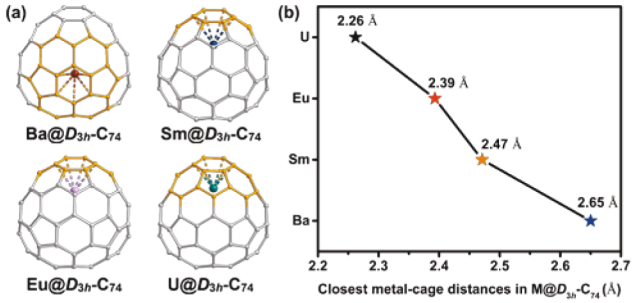

Figure 8. (a) Molecular structures of M@D_{3h}-C_{74} (M = Ba, Sm, Eu, and U) showing the differences of metal positions. (b) The closest metal−cage distances for M@D_{3h}-C_{74} (M = Ba, Sm, Eu, and U).

located on the same symmetry plane, U is more precisely located over the center of a sumanene-type hexagon, while Eu and Sm shift to a neighboring [6, 6] bond and Ba is adjacent to an *s*-indacene-type hexagon far away from the sumanene-type hexagon and close to the C_3 axis of the D_{3h}-C_{74} cage. Furthermore, the U ion is much closer to the cage's inner surface than the other metal ions, displaying the shortest metal−cage distances and thus the strongest metal−cage interactions.

DFT Study. To better understand the interaction between the uranium ions and the carbon cages and the role of symmetry in the location of the U inside the fullerenes, we have explored the lowest-energy uranium sites for the four new monometallic EMFs displayed in Figure 4. U and also Th tend to formally possess oxidation states of 4+ or 3+ depending on whether the fullerene cage encapsulates one[33−39] or two[52,53] metals. For the smallest fullerene, U@C_s(6)-C_{82}, the three lowest-energy positions for the U ion are located on the plane of symmetry of the carbon cage, the most favored one being that where U interacts with a phenalene (site A in Figure 9a). These results agree with the highest-occupied position identified in the single-crystal X-ray diffraction data. The other two energetically less favored sites are associated with interactions to *as*-indacene and sumanene motifs (sites B and C, respectively, in Figure 9a). All other positions away from the symmetry plane are somewhat higher in energy at a hybrid PBE0 level (see Table 1). A similar trend can be observed at a GGA PBE level (Table S3).

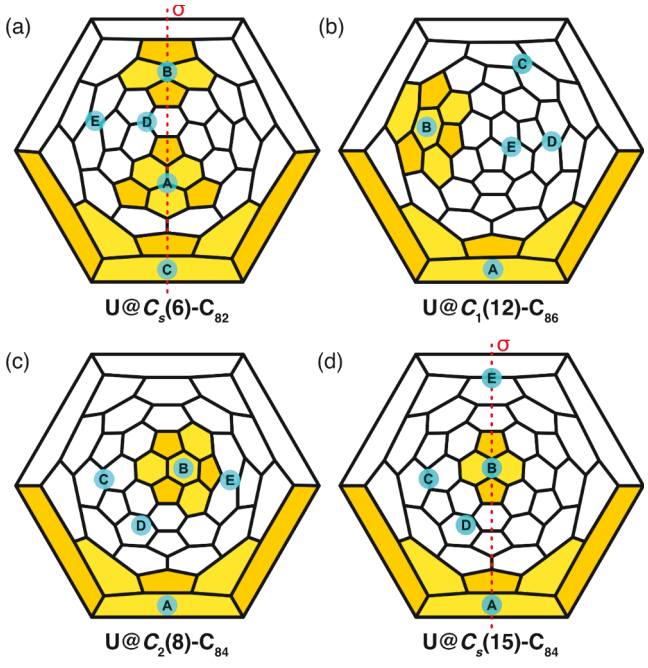

Figure 9. Schlegel diagrams for four uranium endohedral fullerenes. Letters represent the computed uranium sites (see Table 1). Most stable sites have their patterns highlighted.

Table 1. Relative Energies Computed for Different U Sites for Four Monometallic Uranium Endohedral Metallofullerenes[a]

site	U@C_s(6)-C_{82}	U@C1(12)-C_{86}	U@C_2(8)-C_{84}	U@C_s(15)-C_{84}
A	0.0	0.0	0.0	0.0
B	2.1	5.2	0.0	14.6
C	5.1	20.6	24.1	19.5
D	5.2	21.2	36.6	22.4
E	9.4	31.3	27.5	33.4

[a]For a representation of the uranium sites see Figure 9. Relative energies computed at the hybrid PBE0 level are in kcal mol^{-1}. See also Table S3 for GGA PBE values.

Patterns such as phenalene, sumanene, or *as*-indacene (Scheme 1) have been shown to be particularly stabilizing for uranium endohedral metallofullerenes and other metals,[47,54] both for cages with and without symmetry planes. These patterns have a local inherent symmetry, such as C_{3v} for sumanene and phenalene or C_{2v} for *as*-indacene, which usually share one of the symmetry planes of the whole cage. This means, for example, that for fullerenes containing a symmetry plane and a unique sumanene (or a phenalene), these motifs will necessarily share the symmetry plane of the molecule. Indeed, Figure 9a and d show that the most stable sites for isomers C_s(6)-C_{82} (A, B, and C) and C_s(15)-C_{84} (A and B) are for patterns placed on the symmetry plane. It is interesting to point out that the energy range for the different sites for C_s(6)-C_{82} (Table 1) is significantly smaller than for C_s(15)-C_{84}, where site A next to a sumanene is clearly favored.

Two monometallic EMFs with 84 C atoms have been analyzed, i.e., isomers 8 and 15 with carbon cages of C_2 and C_s symmetries, respectively. For U@C_2(8)-C_{84}, two symmetry-related low-energy sites with the uranium atom in contact with a sumanene (sites A and B in Figure 9c) were found to be significantly more stable than the rest of the sites (Table 1). U@C_s(15)-C_{84} is related to U@C_2(8)-C_{84} by a Stone−Wales transformation, highlighted in Figure 10. This simple transformation does generate a symmetry plane on the carbon cage, which at the same time destroys one of the sumanene patterns, forming an *as*-indacene pattern instead. A direct consequence of all of these transformations is the displacement of the uranium site toward the symmetry plane. Nevertheless, this position increases significantly in energy (see Table 1). The most stable site is still on a sumanene, in agreement with the occupancy of U determined by X-ray single-crystal diffraction. Sites outside of the symmetry plane tend to be less stable. Interestingly, U@C_s(15)-C_{86} and U@C_1(11)-C_{86} show the same kind of relationship (Figure S7).

Finally, we have also analyzed the U@C_1(12)-C_{86} system, which is predicted to be among the most abundant IPR isomers at high temperatures, below the most favorable U@C_1(11)-C_{86} (see molar fractions in Figure S8). Chiral cages with low symmetry (C_1) are favored by thermal and entropic effects at the high synthesis temperatures in the arc reactor

https://doi.org/10.1021/jacs.1c06833
J. Am. Chem. Soc. 2021, 143, 15309−15318

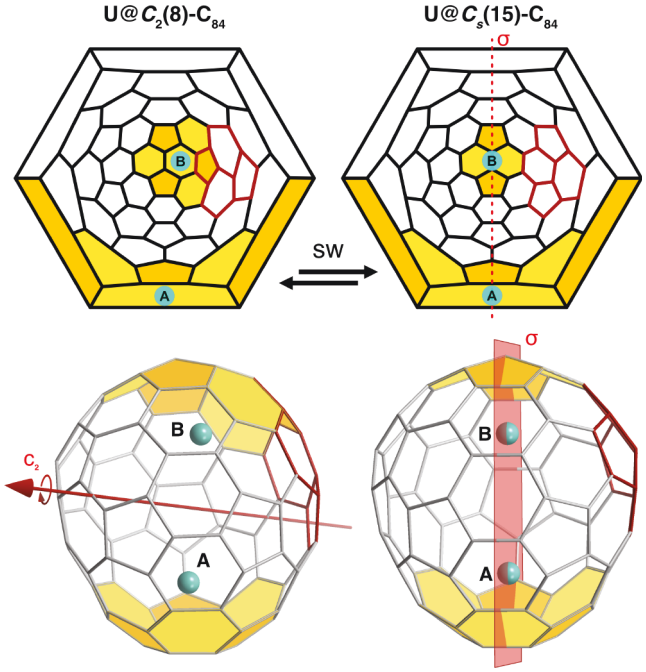

Figure 10. Schlegel diagrams and three-dimensional representations of U@C_2(8)-C_{84} and U@C_s(15)-C_{84}. Both representations show in red the regions where the Stone–Wales transformation occurs to interconvert the structures.

with respect to the more symmetric cages.[37] We observe that the most stable uranium site is at a sumanene (site A in Figure 9b), in agreement with the single-crystal X-ray diffraction structure. The second most stable uranium site for U@C_1(12)-C_{86} is also at a sumanene (site B in Figure 9b), while other positions have higher relative energies. It is worth mentioning that for fullerenes with 86 carbon atoms, 18 out of the 19 IPR isomers have at least one sumanene pattern on their topologies, and 17 out of 18 do show the U atom interacting with the sumanene as their most favorable site. This agrees with previous studies for Th@C_{2n} systems, where sumanene and phenalene patterns show coordination with the encapsulated actinide metal,[47,54] with enhanced covalent and electrostatic interactions. Out of the 19 IPR isomers of U@C_{86}, five possess a symmetry plane, and all of them have the most stable uranium site on the symmetry plane (see Figure S9).

Although U@C_s(16)-C_{86} is not one of the most stable IPR isomers, it represents an interesting case to study. This structure, with a single symmetry plane, contains three sumanene stable sites, one located on the symmetry plane and the other two at both sides of this mirror plane (see Figure S10a). Of these, the most stable uranium site is located on the symmetry plane. The other two sites are 11.4 kcal·mol^{-1} (at a PBE0 level) above the most stable one. This suggests that the mirror plane site is somehow stabilized due to the symmetric structure. Carbon cages having only an *n*-fold axis of rotation might not exhibit the same behavior. As we have seen with U@C_2(8)-C_{84}, positions along the C_2 axis were not found to be significantly stable (see Figure S10b) since they do not allow for an efficient metal–cage interaction. In these symmetries, the X-ray structures could show higher disorder between two or more preferential sites.

A full analysis of all 24 IPR isomers of Th@C_{84} was performed by Straka and co-workers,[55] which showed that 14 out of the 24 IPR isomers contain at least one symmetry plane, and for 10 out of these 14 symmetric cages, the Th atom is located on the symmetry plane. Given that their results are not entirely in agreement with our predictions, we decided to carefully reanalyze the four structures that do not agree, i.e., Th@C_s(14)-C_{84}, Th@C_s(16)-C_{84}, Th@C_s(17)-C_{84}, and Th@C_s(19)-C_{84}. In all four cases, upon further exploration, we have found new lower-energy locations on the symmetry planes (see Figure S11). Therefore, all 14 IPR symmetric cages of Th@C_{84} have their most stable Th sites on the symmetry planes. Other symmetric thorium and uranium EMFs have been studied computationally, and for all of them the metal was found to be located on the mirror plane.[4,34,36,47,54]

CONCLUSIONS

In summary, four new U-based mono-metallofullerenes, U@C_s(6)-C_{82}, U@C_2(8)-C_{84}, U@C_s(15)-C_{84}, and U@C_1(12)-C_{86}, have been successfully synthesized, isolated, and characterized by mass spectrometry, UV–vis–NIR absorption spectroscopy, cyclic voltammetry, and single-crystal X-ray diffractometry. Based on the crystallographic results, showing that the U ions are located on the symmetry planes of C_s(6)-C_{82} and C_s(15)-C_{84}, previously crystallographically characterized mono-metallofullerenes with 30 different kinds of pristine cages were reinvestigated. The results show that most metal ions in fullerenes are located over a [6, 6] bond or the center of a hexagon with respect to some symmetric patterns. The charge transfer is also found to play an essential role in determining the position of the encapsulated metal ions. In addition, the encapsulated metal ions are always located on the symmetry planes of the fullerene cages, as long as the cages are mirror-symmetric. This finding was observed for all the mirror-symmetric mono-metallofullerenes no matter what metal it is, what the cage size is, and what fullerene motif was coordinated with the metal ion.

DFT calculations clearly show that the uranium–fullerene motif interaction determines the stability of the position of the actinide inside the fullerene and that often the most stable site for a U atom is next to a sumanene motif. It is relevant to highlight that in carbon cages containing a symmetry plane, the metal will be located on the symmetry plane, thanks mainly to the inherent local symmetry of the most attractive patterns, which share one of their symmetry planes with the whole fullerene. Furthermore, the metal prefers to occupy a symmetrical arrangement with respect to the interacting motifs. We cannot totally rule out that the most abundant position of the metal in an X-ray structure could sometimes be found outside the plane of symmetry. However, in more than 20 computationally analyzed fullerenes containing at least one symmetry plane, the actinide was found to be located on the mirror plane with no exception. These findings provide a guideline for structural determinations by synergistic crystallographic and theoretical methods so that erroneous structures could be avoided. Besides, they also give new fundamental insights about the metal–cage interactions to further understand the nature of endohedral fullerenes.

EXPERIMENTAL SECTION

Synthesis and Isolation of U@C_{2n} (2*n* = 82–86). Soots containing four new mono-metallofullerenes U@C_{2n} (2*n* = 82–86) were synthesized by the direct-current arc-discharge method under optimized conditions. High-purity graphite rods filled with a mixture of U_3O_8/graphite powder (weight ratio = 1/2) were evaporated in an arcing reactor under a 200 Torr He atmosphere. The resulting soot

https://doi.org/10.1021/jacs.1c06833
J. Am. Chem. Soc. 2021, 143, 15309–15318

was soaked in a CS_2 solution overnight and then extracted in a supersonic cleaner for 1 h. Multiple-stage HPLC procedures were employed to purify the four new compounds.

Spectroscopic Studies. Mass spectra were recorded on a Bruker LRF MALDI-TOF spectrometer using positive-ion mode. UV−vis−NIR absorption spectra of purified U@C_{2n} ($2n$ = 82−86) dissolved in toluene were measured on an Agilent Cary 5000 spectrometer.

Electrochemical Studies. Cyclic voltammetry results were measured on a CH Instruments 600E potentiostat. The conventional three-electrode cell, including a glassy carbon working electrode, a platinum counter electrode, and a silver reference electrode, was employed in a 0.05 M $TBAPF_6$/*o*-DCB solution at a scan rate of 100 mV/s. Ferrocene (Fc) and $TBAPF_6$ were used as the internal standard and supporting electrolyte, respectively.

X-ray Diffraction Analysis. The crystallographic data were collected on a Bruker D8 Venture single-crystal diffractometer equipped with Cu K_α radiation (λ = 1.54184 Å) or Mo K_α radiation (0.71073 Å) below 120 K. The data were reduced with the program APEX 3. The structures were solved and refined using the Olex2 software[56] with SHELXT-2014 by the intrinsic phasing method and SHELXL-2018 by full-matrix least-squares based on F^2.[57] The Squeeze program available in the Platon software was employed to calculate the contribution of severely disordered solvent molecules in the crystal of U@C_2(8)-C_{84}.[58] The supplementary crystallographic data for this paper can be obtained free of charge from the Cambridge Crystallographic Data Centre with CCDC numbers 2067651−2067654 via www.ccdc.cam.ac.uk/data_request/cif.

Computational Details. All calculations were carried out using density functional theory (DFT) with the ADF 2019 package[59] using PBE and PBE0 exchange−correlation functionals. Slater triple-ζ polarization (TZP) basis sets were used to describe the valence electrons of U, Th, and C.[60,61] Frozen cores were described by means of single Slater functions, consisting of the 1s shell for C and the 1s to 5d shells for U and Th. Scalar relativistic corrections were included by means of the ZORA formalism. Dispersion corrections by Grimme were also included.[62] Open-shell calculations were performed at an unrestricted level. Optimizations were performed using the hybrid PBE0 exchange−correlation functional, while frequencies were calculated using the less demanding PBE correlation functional. A data set collection of computational results is available in the ioChem-BD repository and can be accessed via 10.19061/iochem-bd-2-55.[63]

■ ASSOCIATED CONTENT

Supporting Information

The Supporting Information is available free of charge at https://pubs.acs.org/doi/10.1021/jacs.1c06833.

General methods; drawings of HPLC procedures of U@C_{2n} ($2n$ = 82−86) and possible structures of Sm@C_2(40)-C_{90} and Sm@C_2(42)-C_{90}; table of the redox potentials of U@C_{2n} ($2n$ = 74−86); detailed crystallographic information on U@C_{2n} ($2n$ = 82−86); additional DFT results from computations on U@C_{2n} ($2n$ = 82−86) and related systems (PDF)

Accession Codes

CCDC 2067651−2067654 contain the supplementary crystallographic data for this paper. These data can be obtained free of charge via www.ccdc.cam.ac.uk/data_request/cif, or by emailing data_request@ccdc.cam.ac.uk, or by contacting The Cambridge Crystallographic Data Centre, 12 Union Road, Cambridge CB2 1EZ, UK; fax: +44 1223 336033.

■ AUTHOR INFORMATION

Corresponding Authors

Luis Echegoyen − *Department of Chemistry and Biochemistry, University of Texas at El Paso, El Paso, Texas 79968, United States;* orcid.org/0000-0003-1107-9423; Email: echegoyen@utep.edu

Josep M. Poblet − *Departament de Química Física i Inorgànica, Universitat Rovira i Virgili, 43007 Tarragona, Spain;* orcid.org/0000-0002-4533-0623; Email: josepmaria.poblet@urv.cat

Authors

Yang-Rong Yao − *Department of Chemistry and Biochemistry, University of Texas at El Paso, El Paso, Texas 79968, United States;* orcid.org/0000-0003-3495-1691

Yannick Roselló − *Departament de Química Física i Inorgànica, Universitat Rovira i Virgili, 43007 Tarragona, Spain;* orcid.org/0000-0001-9922-1249

Lei Ma − *Department of Chemistry and Biochemistry, University of Texas at El Paso, El Paso, Texas 79968, United States;* orcid.org/0000-0002-8555-5085

Alain Rafael Puente Santiago − *Department of Chemistry and Biochemistry, University of Texas at El Paso, El Paso, Texas 79968, United States;* orcid.org/0000-0002-8491-3565

Alejandro Metta-Magaña − *Department of Chemistry and Biochemistry, University of Texas at El Paso, El Paso, Texas 79968, United States;* orcid.org/0000-0001-9993-8485

Ning Chen − *College of Chemistry, Chemical Engineering and Materials Science, and State Key Laboratory of Radiation Medicine and Protection, Soochow University, Suzhou, Jiangsu 215123, People's Republic of China;* orcid.org/0000-0002-9405-6229

Antonio Rodríguez-Fortea − *Departament de Química Física i Inorgànica, Universitat Rovira i Virgili, 43007 Tarragona, Spain;* orcid.org/0000-0001-5884-5629

Complete contact information is available at: https://pubs.acs.org/10.1021/jacs.1c06833

Author Contributions

[§]Y.-R.Y. and Y.R. contributed equally to this work.

Notes

The authors declare no competing financial interest.

■ ACKNOWLEDGMENTS

L.E. thanks the U.S. National Science Foundation (NSF) for the generous support of this work under grant CHE-1801317, and the Robert A. Welch Foundation is also gratefully acknowledged for an endowed chair to L.E. (grant AH-0033). J.M.P. and A.R.-F. thank the Spanish Ministry of Science (PID2020-112762GB-I00), the Generalitat de Catalunya (2017SGR629), and the URV for support. J.M.P. also thanks the ICREA Foundation for an ICREA ACADEMIA award. N.C. thanks the National Science Foundation China (NSFC 51302178 and 91961109), the NSF of Jiangsu Province (BK20171211), and the Priority Academic Program Development of Jiangsu Higher Education Institutions (PAPD).

■ REFERENCES

(1) Popov, A. A.; Yang, S.; Dunsch, L. Endohedral Fullerenes. *Chem. Rev.* **2013**, *113*, 5989−6113.

(2) Yang, S.; Wei, T.; Jin, F. When metal clusters meet carbon cages: endohedral clusterfullerenes. *Chem. Soc. Rev.* **2017**, *46*, 5005−5058.

(3) Shen, W.; Hu, S.; Lu, X. Endohedral Metallofullerenes: New Structures and Unseen Phenomena. *Chem. - Eur. J.* **2020**, *26*, 5748−5757.

(4) Li, Y.; Yang, L.; Liu, C.; Hou, Q.; Jin, P.; Lu, X. Th-Based Endohedral Metallofullerenes: Anomalous Metal Position and Significant Metal-Cage Covalent Interactions with the Involvement of Th 5f Orbitals. *Inorg. Chem.* **2018**, *57*, 7142−7150.
(5) Wang, K.; Zhao, J.; Yang, S.; Chen, L.; Li, Q.; Wang, B.; Yang, S.; Yang, J.; Hou, J. G.; Zhu, Q. Unveiling Metal-Cage Hybrid States in a Single Endohedral Metallofullerene. *Phys. Rev. Lett.* **2003**, *91*, 185504.
(6) Popov, A. A.; Dunsch, L. Structure, Stability, and Cluster-Cage Interactions in Nitride Clusterfullerenes $M_3N@C_{2n}$ (M = Sc, Y; 2*n* = 68−98): a Density Functional Theory Study. *J. Am. Chem. Soc.* **2007**, *129*, 11835−11849.
(7) Zhang, K.; Wang, C.; Zhang, M.; Bai, Z.; Xie, F.-F.; Tan, Y.-Z.; Guo, Y.; Hu, K.-J.; Cao, L.; Zhang, S.; Tu, X.; Pan, D.; Kang, L.; Chen, J.; Wu, P.; Wang, X.; Wang, J.; Liu, J.; Song, Y.; Wang, G.; Song, F.; Ji, W.; Xie, S.-Y.; Shi, S.-F.; Reed, M. A.; Wang, B. A Gd@C_{82} single-molecule electret. *Nat. Nanotechnol.* **2020**, *15*, 1019−1024.
(8) Heath, J. R.; O'Brien, S. C.; Zhang, Q.; Liu, Y.; Curl, R. F.; Tittel, F. K.; Smalley, R. E. Lanthanum complexes of spheroidal carbon shells. *J. Am. Chem. Soc.* **1985**, *107*, 7779−7780.
(9) Takata, M.; Umeda, B.; Nishibori, E.; Sakata, M.; Saitot, Y.; Ohno, M.; Shinohara, H. Confirmation by X-ray diffraction of the endohedral nature of the metallofullerene Y@C_{82}. *Nature* **1995**, *377*, 46−49.
(10) Olmstead, M. M.; Costa, D. A.; Maitra, K.; Noll, B. C.; Phillips, S. L.; Van Calcar, P. M.; Balch, A. L. Interaction of Curved and Flat Molecular Surfaces. The Structures of Crystalline Compounds Composed of Fullerene (C_{60}, $C_{60}O$, C_{70}, and $C_{120}O$) and Metal Octaethylporphyrin Units. *J. Am. Chem. Soc.* **1999**, *121*, 7090−7097.
(11) Reich, A.; Panthöfer, M.; Modrow, H.; Wedig, U.; Jansen, M. The Structure of Ba@C_{74}. *J. Am. Chem. Soc.* **2004**, *126*, 14428−14434.
(12) Che, Y.; Yang, H.; Wang, Z.; Jin, H.; Liu, Z.; Lu, C.; Zuo, T.; Dorn, H. C.; Beavers, C. M.; Olmstead, M. M.; Balch, A. L. Isolation and Structural Characterization of Two Very Large, and Largely Empty, Endohedral Fullerenes: Tm@C_{3v}-C_{94} and Ca@C_{3v}-C_{94}. *Inorg. Chem.* **2009**, *48*, 6004−6010.
(13) Bao, L.; Pan, C.; Slanina, Z.; Uhlik, F.; Akasaka, T.; Lu, X. Isolation and Crystallographic Characterization of the Labile Isomer of Y@C_{82} Cocrystallized with Ni(OEP): Unprecedented Dimerization of Pristine Metallofullerenes. *Angew. Chem., Int. Ed.* **2016**, *55*, 9234−9238.
(14) Suzuki, M.; Yamada, M.; Maeda, Y.; Sato, S.; Takano, Y.; Uhlík, F.; Slanina, Z.; Lian, Y.; Lu, X.; Nagase, S.; Olmstead, M. M.; Balch, A. L.; Akasaka, T. The Unanticipated Dimerization of Ce@$C_{2v}(9)$-C_{82} upon Co-crystallization with Ni(octaethylporphyrin) and Comparison with Monomeric M@$C_{2v}(9)$-C_{82} (M = La, Sc, and Y). *Chem. - Eur. J.* **2016**, *22*, 18115−18122.
(15) Sato, S.; Nikawa, H.; Seki, S.; Wang, L.; Luo, G.; Lu, J.; Haranaka, M.; Tsuchiya, T.; Nagase, S.; Akasaka, T. A Co-Crystal Composed of the Paramagnetic Endohedral Metallofullerene La@C_{82} and a Nickel Porphyrin with High Electron Mobility. *Angew. Chem., Int. Ed.* **2012**, *51*, 1589−1591.
(16) Suzuki, M.; Lu, X.; Sato, S.; Nikawa, H.; Mizorogi, N.; Slanina, Z.; Tsuchiya, T.; Nagase, S.; Akasaka, T. Where Does the Metal Cation Stay in Gd@$C_{2v}(9)$-C_{82}? A Single-Crystal X-ray Diffraction Study. *Inorg. Chem.* **2012**, *51*, 5270−5273.
(17) Suzuki, M.; Slanina, Z.; Mizorogi, N.; Lu, X.; Nagase, S.; Olmstead, M. M.; Balch, A. L.; Akasaka, T. Single-Crystal X-ray Diffraction Study of Three Yb@C_{82} Isomers Cocrystallized with Ni^{II}(octaethylporphyrin). *J. Am. Chem. Soc.* **2012**, *134*, 18772−18778.
(18) Hu, Z.; Hao, Y.; Slanina, Z.; Gu, Z.; Shi, Z.; Uhlík, F.; Zhao, Y.; Feng, L. Popular C_{82} Fullerene Cage Encapsulating a Divalent Metal Ion Sm^{2+}: Structure and Electrochemistry. *Inorg. Chem.* **2015**, *54*, 2103−2108.
(19) Hu, S.; Liu, T.; Shen, W.; Slanina, Z.; Akasaka, T.; Xie, Y.; Uhlik, F.; Huang, W.; Lu, X. Isolation and Structural Characterization of Er@$C_{2v}(9)$-C_{82} and Er@$C_s(6)$-C_{82}: Regioselective Dimerization of a Pristine Endohedral Metallofullerene Induced by Cage Symmetry. *Inorg. Chem.* **2019**, *58*, 2177−2182.
(20) Zhang, Y.; Guan, R.; Chen, M.; Shen, Y.; Pan, Q.; Lian, Y.; Yang, S. Favorite Orientation of the Carbon Cage and a Unique Two-Dimensional-Layered Packing Model in the Cocrystals of Nd@C_{82}(I,II) Isomers with Decapyrrylcorannulene. *Inorg. Chem.* **2021**, *60*, 1462−1471.
(21) Hao, Y.; Feng, L.; Xu, W.; Gu, Z.; Hu, Z.; Shi, Z.; Slanina, Z.; Uhlík, F. Sm@C_{2v}(19138)-C_{76}: A Non-IPR Cage Stabilized by a Divalent Metal Ion. *Inorg. Chem.* **2015**, *54*, 4243−4248.
(22) Bao, L.; Yu, P.; Pan, C.; Shen, W.; Lu, X. Crystallographic identification of Eu@C_{2n} (2*n* = 88, 86 and 84): completing a transformation map for existing metallofullerenes. *Chem. Sci.* **2019**, *10*, 2153−2158.
(23) Yang, H.; Jin, H.; Wang, X.; Liu, Z.; Yu, M.; Zhao, F.; Mercado, B. Q.; Olmstead, M. M.; Balch, A. L. X-ray Crystallographic Characterization of New Soluble Endohedral Fullerenes Utilizing the Popular C_{82} Bucky Cage. Isolation and Structural Characterization of Sm@$C_{3v}(7)$-C_{82}, Sm@$C_s(6)$-C_{82}, and Sm@$C_2(5)$-C_{82}. *J. Am. Chem. Soc.* **2012**, *134*, 14127−14136.
(24) Bao, L.; Yu, P.; Li, Y.; Pan, C.; Shen, W.; Jin, P.; Liang, S.; Lu, X. Highly regioselective complexation of tungsten with Eu@C_{82}/Eu@C_{84}: interplay between endohedral and exohedral metallic units induced by electron transfer. *Chem. Sci.* **2019**, *10*, 4945−4950.
(25) Yang, H.; Wang, Z.; Jin, H.; Hong, B.; Liu, Z.; Beavers, C. M.; Olmstead, M. M.; Balch, A. L. Isolation and Crystallographic Characterization of Sm@$C_{2v}(3)$-C_{80} Through Cocrystal Formation with NiII(octaethylporphyrin) or Bis(ethylenedithio)-tetrathiafulvalene. *Inorg. Chem.* **2013**, *52*, 1275−1284.
(26) Bao, L.; Li, Y.; Yu, P.; Shen, W.; Jin, P.; Lu, X. Preferential Formation of Mono-Metallofullerenes Governed by the Encapsulation Energy of the Metal Elements: A Case Study on Eu@C_{2n} (2*n* = 74−84) Revealing a General Rule. *Angew. Chem., Int. Ed.* **2020**, *59*, 5259−5262.
(27) Lu, X.; Lian, Y.; Beavers, C. M.; Mizorogi, N.; Slanina, Z.; Nagase, S.; Akasaka, T. Crystallographic X-ray Analyses of Yb@$C_{2v}(3)$-C_{80} Reveal a Feasible Rule That Governs the Location of a Rare Earth Metal inside a Medium-Sized Fullerene. *J. Am. Chem. Soc.* **2011**, *133*, 10772−10775.
(28) Xu, W.; Niu, B.; Shi, Z.; Lian, Y.; Feng, L. Sm@$C_{2v}(3)$-C_{80}: site-hopping motion of endohedral Sm atom and metal-induced effect on redox profile. *Nanoscale* **2012**, *4*, 6876−6879.
(29) Yang, H.; Jin, H.; Zhen, H.; Wang, Z.; Liu, Z.; Beavers, C. M.; Mercado, B. Q.; Olmstead, M. M.; Balch, A. L. Isolation and Crystallographic Identification of Four Isomers of Sm@C_{90}. *J. Am. Chem. Soc.* **2011**, *133*, 6299−6306.
(30) Jin, H.; Yang, H.; Yu, M.; Liu, Z.; Beavers, C. M.; Olmstead, M. M.; Balch, A. L. Single Samarium Atoms in Large Fullerene Cages. Characterization of Two Isomers of Sm@C_{92} and Four Isomers of Sm@C_{94} with the X-ray Crystallographic Identification of Sm@$C_1(42)$-C_{92}, Sm@$C_s(24)$-C_{92}, and Sm@$C_{3v}(134)$-C_{94}. *J. Am. Chem. Soc.* **2012**, *134*, 10933−10941.
(31) Zhang, W.; Suzuki, M.; Xie, Y.; Bao, L.; Cai, W.; Slanina, Z.; Nagase, S.; Xu, M.; Akasaka, T.; Lu, X. Molecular Structure and Chemical Property of a Divalent Metallofullerene Yb@$C_2(13)$-C_{84}. *J. Am. Chem. Soc.* **2013**, *135*, 12730−12735.
(32) Xu, W.; Hao, Y.; Uhlik, F.; Shi, Z.; Slanina, Z.; Feng, L. Structural and electrochemical studies of Sm@D_{3h}-C_{74} reveal a weak metal−cage interaction and a small band gap species. *Nanoscale* **2013**, *5*, 10409−10413.
(33) Jin, M.; Zhuang, J.; Wang, Y.; Yang, W.; Liu, X.; Chen, N. Th@T_d(19151)-C_{76}: A Highly Symmetric Fullerene Cage Stabilized by a Tetravalent Actinide Metal Ion. *Inorg. Chem.* **2019**, *58*, 16722−16726.
(34) Wang, Y.; Morales-Martínez, R.; Zhang, X.; Yang, W.; Wang, Y.; Rodríguez-Fortea, A.; Poblet, J. M.; Feng, L.; Wang, S.; Chen, N. Unique Four-Electron Metal-to-Cage Charge Transfer of Th to a C_{82} Fullerene Cage: Complete Structural Characterization of Th@$C_{3v}(8)$-C_{82}. *J. Am. Chem. Soc.* **2017**, *139*, 5110−5116.
(35) Wang, Y.; Morales-Martínez, R.; Cai, W.; Zhuang, J.; Yang, W.; Echegoyen, L.; Poblet, J. M.; Rodríguez-Fortea, A.; Chen, N. Th@

$C_1(11)$-C_{86}: an actinide encapsulated in an unexpected C_{86} fullerene cage. *Chem. Commun.* **2019**, *55*, 9271−9274.
(36) Cai, W.; Morales-Martínez, R.; Zhang, X.; Najera, D.; Romero, E. L.; Metta-Magaña, A.; Rodríguez-Fortea, A.; Fortier, S.; Chen, N.; Poblet, J. M.; Echegoyen, L. Single crystal structures and theoretical calculations of uranium endohedral metallofullerenes ($U@C_{2n}$, $2n$ = 74, 82) show cage isomer dependent oxidation states for U. *Chem. Sci.* **2017**, *8*, 5282−5290.
(37) Cai, W.; Abella, L.; Zhuang, J.; Zhang, X.; Feng, L.; Wang, Y.; Morales-Martínez, R.; Esper, R.; Boero, M.; Metta-Magaña, A.; Rodríguez-Fortea, A.; Poblet, J. M.; Echegoyen, L.; Chen, N. Synthesis and Characterization of Non-Isolated-Pentagon-Rule Actinide Endohedral Metallofullerenes $U@C_1(17418)$-C_{76}, $U@C_1(28324)$-C_{80}, and $Th@C_1(28324)$-C_{80}: Low-Symmetry Cage Selection Directed by a Tetravalent Ion. *J. Am. Chem. Soc.* **2018**, *140*, 18039−18050.
(38) Cai, W.; Alvarado, J.; Metta-Magaña, A.; Chen, N.; Echegoyen, L. Interconversions between Uranium Mono-metallofullerenes: Mechanistic Implications and Role of Asymmetric Cages. *J. Am. Chem. Soc.* **2020**, *142*, 13112−13119.
(39) Yan, Y.; Morales-Martínez, R.; Zhuang, J.; Yao, Y.-R.; Li, X.; Poblet, J. M.; Rodríguez-Fortea, A.; Chen, N. $Th@D_{5h}(6)$-C_{80}: a highly symmetric fullerene cage stabilized by a single metal ion. *Chem. Commun.* **2021**, *57*, 6624−6627.
(40) Lu, X.; Nakajima, K.; Iiduka, Y.; Nikawa, H.; Mizorogi, N.; Slanina, Z.; Tsuchiya, T.; Nagase, S.; Akasaka, T. Structural Elucidation and Regioselective Functionalization of An Unexplored Carbide Cluster Metallofullerene $Sc_2C_2@C_s(6)$-C_{82}. *J. Am. Chem. Soc.* **2011**, *133*, 19553−19558.
(41) Mercado, B. Q.; Stuart, M. A.; Mackey, M. A.; Pickens, J. E.; Confait, B. S.; Stevenson, S.; Easterling, M. L.; Valencia, R.; Rodríguez-Fortea, A.; Poblet, J. M.; Olmstead, M. M.; Balch, A. L. $Sc_2(\mu_2$-O) Trapped in a Fullerene Cage: The Isolation and Structural Characterization of $Sc_2(\mu_2$-O)$@C_s(6)$-C_{82} and the Relevance of the Thermal and Entropic Effects in Fullerene Isomer Selection. *J. Am. Chem. Soc.* **2010**, *132*, 12098−12105.
(42) Mercado, B. Q.; Chen, N.; Rodríguez-Fortea, A.; Mackey, M. A.; Stevenson, S.; Echegoyen, L.; Poblet, J. M.; Olmstead, M. M.; Balch, A. L. The Shape of the $Sc_2(\mu_2$-S) Unit Trapped in C_{82}: Crystallographic, Computational, and Electrochemical Studies of the Isomers, $Sc_2(\mu_2$-S)$@C_s(6)$-C_{82} and $Sc_2(\mu_2$-S)$@C_{3v}(8)$-C_{82}. *J. Am. Chem. Soc.* **2011**, *133*, 6752−6760.
(43) Shen, W.; Bao, L.; Wu, Y.; Pan, C.; Zhao, S.; Fang, H.; Xie, Y.; Jin, P.; Peng, P.; Li, F.-F.; Lu, X. $Lu_2@C_{2n}$ ($2n$ = 82, 84, 86): Crystallographic Evidence of Direct Lu−Lu Bonding between Two Divalent Lutetium Ions Inside Fullerene Cages. *J. Am. Chem. Soc.* **2017**, *139*, 9979−9984.
(44) Hu, S.; Shen, W.; Yang, L.; Duan, G.; Jin, P.; Xie, Y.; Akasaka, T.; Lu, X. Crystallographic and Theoretical Investigations of $Er_2@C_{2n}$ ($2n$ = 82, 84, 86): Indication of Distance-Dependent Metal−Metal Bonding Nature. *Chem. - Eur. J.* **2019**, *25*, 11538−11544.
(45) Pan, C.; Shen, W.; Yang, L.; Bao, L.; Wei, Z.; Jin, P.; Fang, H.; Xie, Y.; Akasaka, T.; Lu, X. Crystallographic characterization of Y_2C_{2n} ($2n$ = 82, 88−94): direct Y−Y bonding and cage-dependent cluster evolution. *Chem. Sci.* **2019**, *10*, 4707−4713.
(46) Hu, S.; Zhao, P.; Shen, W.; Ehara, M.; Xie, Y.; Akasaka, T.; Lu, X. Crystallographic Characterization of $Er_2C_2@C_{80-88}$: Cluster Stretching with Cage Elongation. *Inorg. Chem.* **2020**, *59*, 1940−1946.
(47) Li, Y.; Yang, L.; Wei, Z.; Hou, Q.; Li, L.; Jin, P. Robust metal-pentagon interactions in the Th-based endohedral metallofullerenes revealed by DFT calculations. *Int. J. Quantum Chem.* **2019**, *119*, e25826.
(48) Kroto, H. W. The stability of the fullerenes C_n, with n = 24, 28, 32, 36, 50, 60 and 70. *Nature* **1987**, *329*, 529−531.
(49) Nakagawa, A.; Nishino, M.; Niwa, H.; Ishino, K.; Wang, Z.; Omachi, H.; Furukawa, K.; Yamaguchi, T.; Kato, T.; Bandow, S.; Rio, J.; Ewels, C.; Aoyagi, S.; Shinohara, H. Crystalline functionalized endohedral C_{60} metallofullerides. *Nat. Commun.* **2018**, *9*, 3073.
(50) Wang, Z.; Aoyagi, S.; Omachi, H.; Kitaura, R.; Shinohara, H. Isolation and Structure Determination of a Missing Endohedral Fullerene $La@C_{70}$ through In Situ Trifluoromethylation. *Angew. Chem., Int. Ed.* **2016**, *55*, 199−202.
(51) Wakahara, T.; Nikawa, H.; Kikuchi, T.; Nakahodo, T.; Rahman, G. M. A.; Tsuchiya, T.; Maeda, Y.; Akasaka, T.; Yoza, K.; Horn, E.; Yamamoto, K.; Mizorogi, N.; Slanina, Z.; Nagase, S. $La@C_{72}$ Having a Non-IPR Carbon Cage. *J. Am. Chem. Soc.* **2006**, *128*, 14228−14229.
(52) Zhang, X.; Wang, Y.; Morales-Martínez, R.; Zhong, J.; de Graaf, C.; Rodríguez-Fortea, A.; Poblet, J. M.; Echegoyen, L.; Feng, L.; Chen, N. $U_2@I_h(7)$-C_{80}: Crystallographic Characterization of a Long-Sought Dimetallic Actinide Endohedral Fullerene. *J. Am. Chem. Soc.* **2018**, *140*, 3907−3915.
(53) Zhuang, J.; Morales-Martínez, R.; Zhang, J.; Wang, Y.; Yao, Y.-R.; Pei, C.; Rodríguez-Fortea, A.; Wang, S.; Echegoyen, L.; de Graaf, C.; Poblet, J. M.; Chen, N. Characterization of a strong covalent Th^{3+}-Th^{3+} bond inside an $I_h(7)$-C_{80} fullerene cage. *Nat. Commun.* **2021**, *12*, 2372.
(54) Jin, P.; Liu, C.; Li, Y.; Li, L.; Zhao, Y. $Th@C_{76}$. Computational characterization of larger actinide endohedral fullerenes. *Int. J. Quantum Chem.* **2018**, *118*, e25501.
(55) Kaminský, J.; Vícha, J.; Bouř, P.; Straka, M. Properties of the Only Thorium Fullerene, $Th@C_{84}$, Uncovered. *J. Phys. Chem. A* **2017**, *121*, 3128−3135.
(56) Dolomanov, O. V.; Bourhis, L. J.; Gildea, R. J.; Howard, J. A. K.; Puschmann, H. OLEX2: a complete structure solution, refinement and analysis program. *J. Appl. Crystallogr.* **2009**, *42*, 339−341.
(57) Sheldrick, G. Crystal structure refinement with SHELXL. *Acta Crystallogr., Sect. C: Struct. Chem.* **2015**, *71*, 3−8.
(58) Spek, A. Structure validation in chemical crystallography. *Acta Crystallogr., Sect. D: Biol. Crystallogr.* **2009**, *65*, 148−155.
(59) te Velde, G.; Bickelhaupt, F. M.; Baerends, E. J.; Fonseca Guerra, C.; van Gisbergen, S. J. A.; Snijders, J. G.; Ziegler, T. Chemistry with ADF. *J. Comput. Chem.* **2001**, *22*, 931−967.
(60) Becke, A. D. Completely numerical calculations on diatomic molecules in the local-density approximation. *Phys. Rev. A: At., Mol., Opt. Phys.* **1986**, *33*, 2786−2788.
(61) Chai, J.-D.; Head-Gordon, M. Long-range corrected hybrid density functionals with damped atom−atom dispersion corrections. *Phys. Chem. Chem. Phys.* **2008**, *10*, 6615−6620.
(62) Grimme, S.; Ehrlich, S.; Goerigk, L. Effect of the damping function in dispersion corrected density functional theory. *J. Comput. Chem.* **2011**, *32*, 1456−1465.
(63) Álvarez-Moreno, M.; de Graaf, C.; López, N.; Maseras, F.; Poblet, J. M.; Bo, C. Managing the Computational Chemistry Big Data Problem: The ioChem-BD Platform. *J. Chem. Inf. Model.* **2015**, *55*, 95−103.

https://doi.org/10.1021/jacs.1c06833
J. Am. Chem. Soc. 2021, 143, 15309−15318